

Sudden change of the photon output field marks phase transitions in the quantum Rabi model

Ye-Hong Chen^{1,2,3}, Yuan Qiu^{1,2}, Adam Miranowicz^{3,4}, Neill Lambert³, Wei Qin³, Roberto Stassi^{3,5}, Yan Xia^{1,2}, Shi-Biao Zheng^{1,2} & Franco Nori^{3,6,7}

The experimental observation of quantum phase transitions predicted by the quantum Rabi model in quantum critical systems is usually challenging due to the lack of signature experimental observables associated with them. Here, we describe a method to identify the dynamical critical phenomenon in the quantum Rabi model consisting of a three-level atom and a cavity at the quantum phase transition. Such a critical phenomenon manifests itself as a sudden change of steady-state output photons in the system driven by two classical fields, when both the atom and the cavity are initially unexcited. The process occurs as the high-frequency pump field is converted into the low-frequency Stokes field and multiple cavity photons in the normal phase, while this conversion cannot occur in the superradiant phase. The sudden change of steady-state output photons is an experimentally accessible measure to probe quantum phase transitions, as it does not require preparing the equilibrium state.

¹Fujian Key Laboratory of Quantum Information and Quantum Optics, Fuzhou University, Fuzhou 350116, China. ²Department of Physics, Fuzhou University, Fuzhou 350116, China. ³Theoretical Quantum Physics Laboratory, RIKEN Cluster for Pioneering Research, Wako-shi, Saitama 351-0198, Japan. ⁴Institute of Spintronics and Quantum Information, Faculty of Physics, Adam Mickiewicz University, 61-614 Poznań, Poland. ⁵Dipartimento di Scienze Matematiche e Informatiche, Scienze Fisiche e Scienze della Terra, Università di Messina, 98166 Messina, Italy. ⁶Quantum Information Physics Theory Research Team, RIKEN Center for Quantum Computing, Wako-shi, Saitama 351-0198, Japan. ⁷Department of Physics, University of Michigan, Ann Arbor, MI 48109-1040, USA. ✉email: yehong.chen@fzu.edu.cn; xia-208@163.com; fnori@riken.jp

In quantum systems close to critical points, small variations of physical parameters can lead to drastic changes in the equilibrium-state properties^{1–4}. An interesting class of quantum critical systems is provided by light-matter interaction models^{5–8}, such as the quantum Rabi^{9,10} and Dicke models^{11–18} describing the interaction of single or many two-level atoms (atomic levels $|g\rangle$ and $|e\rangle$) with a single-model cavity. The quantum Dicke model exhibits a superradiant quantum phase transition (QPT) in the thermodynamic limit of infinite atoms^{11–17}. Such a thermodynamic limit leads to some difficulties in experimentally exploring the superradiant QPTs^{19–26}. Instead, by replacing the thermodynamic limit with a scaling of the system parameters, the quantum Rabi model described by the Hamiltonian (hereafter $\hbar = 1$)

$$H_R = \omega a^\dagger a (|e\rangle\langle e| + |g\rangle\langle g|) + \Omega |e\rangle\langle e| - g(a + a^\dagger)(|g\rangle\langle e| + |e\rangle\langle g|), \quad (1)$$

can also exhibit a superradiant QPT^{9,10}, where ω (Ω) is the cavity-mode (atomic-transition) frequency, a (a^\dagger) is the cavity-mode annihilation (creation) operator, and g is the light-matter coupling strength. We assume that the level frequency of the atomic state $|g\rangle$ is zero. This superradiant QPT has been experimentally observed^{27,28} and is attracting increasing attention^{29–34}. However, one of the most important critical phenomena in this system, i.e., a discontinuity of the derivative for the number of bare photons at the critical point, is hard to observe.

Unlike classical phase transitions, superradiant QPTs can occur when changing the system parameters at zero temperature^{5,6,16}. Specifically, when g approaches the critical point, it was predicted¹⁰ that the mean photon number in the ground eigenstate of H_R suddenly increases to infinity. This corresponds to a QPT from a normal phase (NP), where the ground state of the cavity field is not occupied, to a superradiant phase (SP), where the ground state is macroscopically occupied. However, experimentally exploring this critical phenomenon is challenging because: (i) the time required to prepare this equilibrium state diverges¹⁰; and (ii) these photons are virtual, so cannot be directly measured^{7,8}. Especially, the difficulty (i) may make transition-edge sensing protocols^{35–37} not effective in detecting this kind of phase transitions.

Here we show how to overcome these problems by introducing additional low-energy levels in the quantum Rabi model and driving transitions among these levels. We show that the stimulated emission effect of the whole system can directly reflect the change of the photon-number distributions of the quantum Rabi Hamiltonian. The process can be interpreted as a multi-photon down-conversion induced by stimulated Raman transitions (i.e., a pump photon is converted into a Stokes photon and multiple cavity photons, as shown in Fig. 1a)^{38–41}. This parametric down-conversion process changes abruptly when the superradiant QPT occurs in the quantum Rabi Hamiltonian. Such a change can be observed by measuring the real photons continuously released from the cavity. Note that this parametric down-conversion process was initially studied by Huang et al. in 2014 for photon emission via vacuum-dressed intermediate states³⁹. We find that such a photon emission can be useful in observing quantum critical phenomena. We predict that the steady-state output photon rate can reach $\Phi_{\text{out}}^{\text{ss}} \sim 4 \times 10^{-3} \omega$ in the NP, then suddenly vanishes when tuning the Rabi Hamiltonian into the SP. This demonstrates a sudden change of the ground eigenstate of the quantum Rabi Hamiltonian, and indicates the occurrence of the superradiant QPT.

Superradiant quantum phase transitions

Note that the theory of the superradiant phase transition in the quantum Rabi model was developed first in 2013⁹ and then in 2015¹⁰. For clarity, we first review the theory of the superradiant phase transition in the quantum Rabi model. In the limit of $\Omega/\omega \rightarrow \infty$, following refs. ^{9,10}, we can solve the Hamiltonian H_R in Eq. (1) using a Schrieffer-Wolff transformation^{1,2}:

$$U_{\text{SW}} = \exp\left[\left(\frac{g}{\Omega}\right)(a + a^\dagger)(|e\rangle\langle g| - |g\rangle\langle e|)\right]. \quad (2)$$

For the transformed Hamiltonian, the transitions between the ground- and excited-qubit-state subspaces $\{|n\rangle|g\rangle\}$ and $\{|n\rangle|e\rangle\}$ are negligible. Thus, we perform a projection $\langle g|U_{\text{SW}}^\dagger H_R U_{\text{SW}}|g\rangle$, resulting in

$$H_{\text{np}} = \omega a^\dagger a - \frac{\omega g_c^2}{4}(a + a^\dagger)^2 + O(g_c^2 \omega / \Omega), \quad (3)$$

where

$$g_c = 2g/\sqrt{\omega\Omega},$$

is the normalized coupling strength and $O(g_c^2 \omega / \Omega)$ denotes negligible higher-order terms. The excitation energy of H_{np} is

$$\epsilon_{\text{np}} = \omega \sqrt{1 - g_c^2},$$

which is real only for $g_c \leq 1$ and vanishes at $g_c = 1$, i.e., in the NP¹⁰. The ground eigenstate of H_{np} is $|E_0\rangle = S(r_{\text{np}})|0\rangle$, with

$$S(r_{\text{np}}) = \exp\left[\frac{r_{\text{np}}}{2}(a^\dagger - a)^2\right], \quad \text{and} \quad r_{\text{np}} = -\frac{1}{4} \ln(1 - g_c^2). \quad (4)$$

For $g_c > 1$ and

$$\alpha = \frac{1}{2} \sqrt{\frac{\Omega}{\omega}(g_c^2 - g_c^{-2})} \geq 0, \quad (5)$$

after displacing the cavity field with displacement operators

$$D(\pm\alpha) = \exp[\pm\alpha(a^\dagger - a)], \quad (6)$$

we can employ the same procedure in deriving H_{np} to obtain the Hamiltonian in the SP:

$$H_{\text{sp}} \approx \omega a^\dagger a - \frac{\omega}{4g_c^4}(a + a^\dagger)^2 + \frac{\Omega}{2}(1 - g_c^2) + \omega\alpha^2. \quad (7)$$

The excitation energy of H_{sp} is $\epsilon_{\text{sp}} = \omega \sqrt{1 - g_c^{-4}}$ and the ground eigenstate of H_{sp} is $S(r_{\text{sp}})|0\rangle$, with

$$r_{\text{sp}} = -\frac{1}{4} \ln(1 - g_c^{-4}). \quad (8)$$

Thus, in the lab frame, H_R has two degenerate ground eigenstates

$$|E_0\rangle = D(\pm\alpha)S(r_{\text{sp}})|0\rangle|\downarrow\rangle_{\pm}, \quad (9)$$

where $|\downarrow\rangle_{\pm}$ are the ground eigenstates of

$$H_{\pm} = \Omega|e\rangle\langle e| \mp 2g\alpha(|e\rangle\langle g| + |g\rangle\langle e|). \quad (10)$$

This is because two different displacement parameters $\pm\alpha$ result in an identical spectrum⁹.

Demonstrating the critical phenomenon

The sudden change of $\bar{n}_0 = \langle E_0|a^\dagger a|E_0\rangle$ at the critical point $g_c = 1$ is the most important benchmark of the superradiant QPT. Specifically, when $\Omega/\omega \rightarrow \infty$, the derivative $d\bar{n}_0/dg_c$ is discontinuous at the critical point $g_c = 1$ (see Fig. 2a), indicating the occurrence of the superradiant QPT. However, observing this critical phenomenon is still challenging in experiments mainly because: (i) it is difficult to prepare the ground state $|E_0\rangle$ at the critical point; (ii) one cannot adiabatically tune control parameters across the critical point^{27,28} since the energy gap mostly

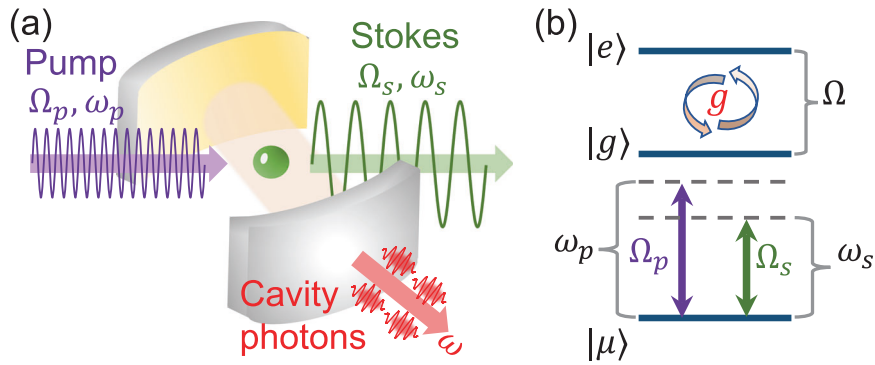


Fig. 1 Sketch and atomic level structure of the protocol. **a** Sketch of the parametric down-conversion process in an atom-cavity system. A pump pulse of frequency ω_p is converted into a Stokes pulse of frequency ω_s and multiple cavity photons of frequency ω . **b** Level structure of the atom. The upper two atomic levels $|g\rangle$ and $|e\rangle$ are ultrastrongly coupled to the cavity mode with strength g . The lower two levels $|g\rangle$ and $|\mu\rangle$ are off-resonantly driven by a composite pulse of two frequencies (ω_p and ω_s) and two amplitudes (Ω_p and Ω_s).

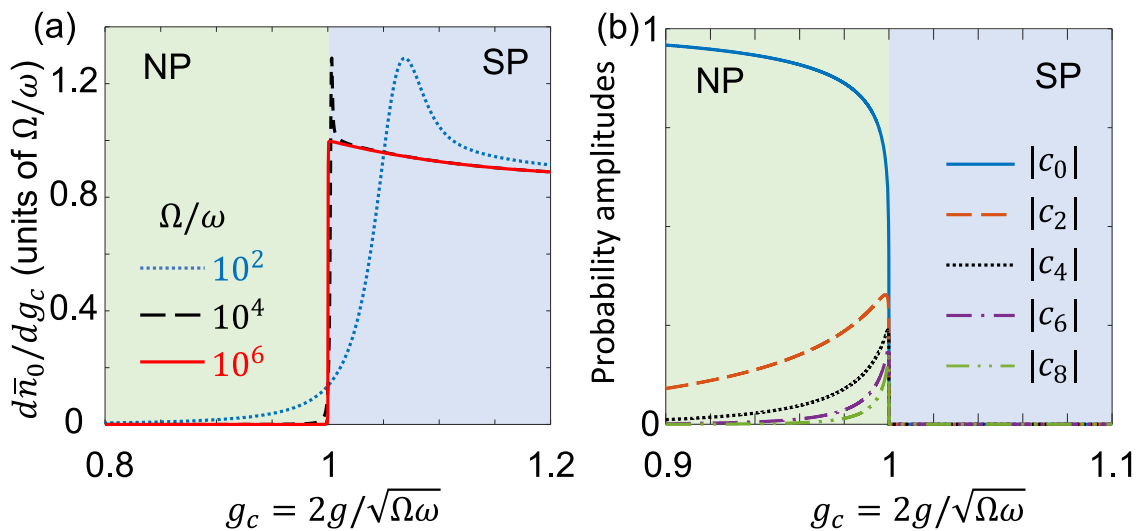


Fig. 2 Sudden change of photon number distribution. **a** Derivative $d\bar{n}_0/dg_c$ of the virtual cavity excitation number $\bar{n}_0 = \langle E_0|a^\dagger a|E_0\rangle$ calculated for different frequency rate Ω/ω . **b** Probability amplitudes $|c_{2k}|$ of the states $|2k\rangle|g\rangle$ in the eigenstate $|E_0\rangle$ of H_R in Eq. (1) when $\Omega = 10^6\omega$ approximately satisfying the condition $\Omega/\omega \rightarrow \infty$. The green- and blue-shaded areas denote the normal phase (NP) and the superradiant phase (SP), respectively.

closes at the critical point; and (iii) the photons in the ground eigenstate $|E_0\rangle$ are virtual and cannot be directly measured^{7,8}.

Instead, in this manuscript, we propose to measure the sudden change of the photon number distributions of $|E_0\rangle$, i.e., the probability amplitudes $c_k(g_c) = \langle g| \langle k|E_0\rangle$. This is equivalent to measuring the change of $\langle E_0|a^\dagger a|E_0\rangle$ because it can be calculated using the photon number distributions. In the $\Omega/\omega \rightarrow \infty$ limit, it is expected that $\alpha \rightarrow \infty$ and $r_{sp} \neq 0$ when $g_c > 1$. Thus, when g_c is tuned across the critical point, there is a sudden change in the amplitude c_{2k} :

$$|c_{2k}(g_c)| \xrightarrow{g_c=1^-} \left| \frac{[-\tanh(r_{np})]^k \sqrt{(2k)!}}{2^k k! \sqrt{\cosh(r_{np})}} \right| > 0,$$

$$|c_{2k}(g_c)| \xrightarrow{g_c=1^+} \left| \frac{(\tanh r_{sp})^k \exp\left[-\frac{\alpha^2}{2}(1 + \tanh r_{sp})\right] \mathcal{H}_n(x)}{2^k \sqrt{(2k)! \cosh r_{sp}}} \right| \rightarrow 0,$$
(11)

where $\mathcal{H}_n(x)$ are the Hermite polynomials with

$$x = \frac{\alpha \exp(r_{sp})}{\sqrt{\sinh 2r_{sp}}}. \quad (12)$$

Such a change is obvious when k is small, because $|c_{2k}(g_c \rightarrow 1^-)|$ is significant as shown in Fig. 2b. Especially, for $k < 5$, the components of the few-photon states in the eigenstate $|E_0\rangle$ of H_R suddenly vanish when g_c is tuned across the critical point (see Fig. 2b). This coincides with the sudden changes of the photon number \bar{n}_0 and its derivative $d\bar{n}_0/dg_c$ (see the red-solid curve in Fig. 2a).

To demonstrate the sudden change of c_{2k} , following the idea in ref. ³⁹, we introduce a third low-energy level $|\mu\rangle$ with level frequency $\omega_\mu < 0$ for the atom (see Fig. 1b). We assume that $|\omega_\mu| \gg \omega$, so that the state $|\mu\rangle$ is far off-resonance to the cavity bare frequency. The atom-cavity interaction becomes

$$H_0 = H_R + \omega_\mu |\mu\rangle\langle\mu| + \omega a^\dagger a |\mu\rangle\langle\mu|, \quad (13)$$

whose eigenstates $|\xi_i\rangle$ can be separated into: (i) the noninteracting sectors $|\mu_n\rangle = |n\rangle|\mu\rangle$ with eigenvalues $n\omega + \omega_\mu$; and (ii) the

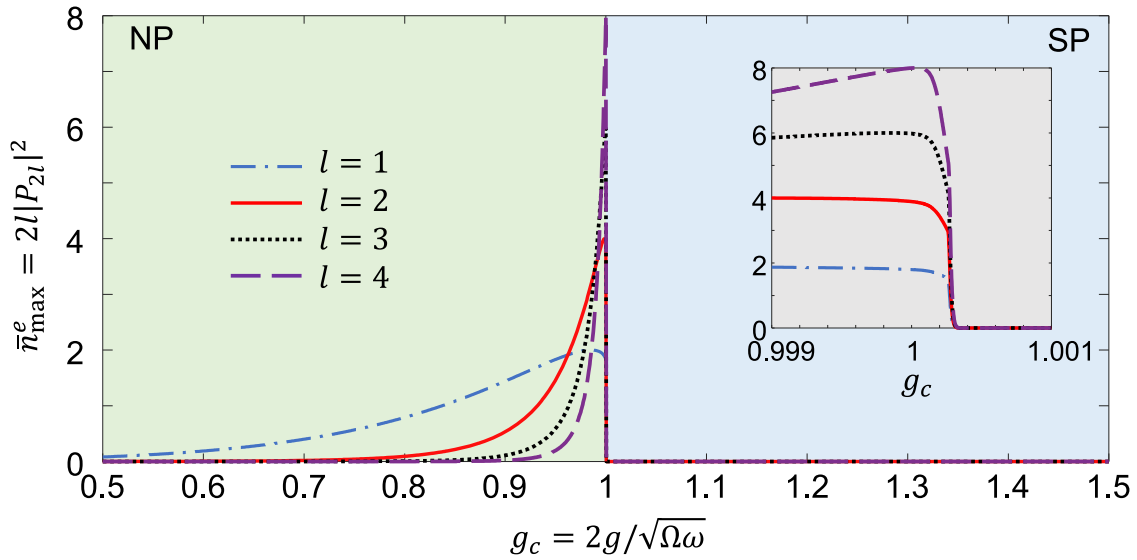


Fig. 3 Critical phenomenon. Theoretical prediction of the maximum photon number of the system after a finite-time evolution, according to Eqs. (16) and (17). For $\Xi \rightarrow 0$, we impose $t = 10^6/\omega$ when $\pi/\Xi \rightarrow \infty$, to avoid an infinite evolution time in the coherent dynamics. Parameters are: $\Omega = 10^6\omega$, $\omega_\mu = E_0 - [2(n_d - l) + 0.25]\omega$, $\Omega_p = 0.005(E_2 - E_0)$, and $\Omega_s = 2\Omega_p$. For simplicity, we choose $n_d = 2 + l$ in the simulation.

eigenstates $|E_m\rangle$ of H_R with eigenvalues E_m ($j, n, m = 0, 1, 2, \dots$). The ground state of the whole system becomes $|\mu_0\rangle$, which is the initial state for the system dynamics hereafter.

Then, as shown in Fig. 1, we employ a composite pulse to drive the atomic transition $|\mu\rangle \leftrightarrow |g\rangle$:

$$H_D = [\Omega_p \cos(\omega_p t) + \Omega_s \cos(\omega_s t)] (|\mu\rangle\langle g| + |g\rangle\langle \mu|), \quad (14)$$

where $\Omega_{p,(s)}$ and $\omega_{p,(s)}$ are the driving amplitude and frequency, respectively. Focusing on the changes of few-photon components ($k < 5$), we choose $\omega_p = E_0 - \omega_\mu$ and $\omega_s = E_0 - \omega_\mu - 2l\omega$, for $l = 1, 2, \dots$, resulting in the resonant transitions $|\mu_0\rangle \leftrightarrow |E_0\rangle \leftrightarrow |\mu_{2l}\rangle$ in the subspace $\{|\xi_j\rangle\}$. Specifically, for weak drivings $\Omega_{p,(s)} \ll |E_2 - E_0|$, the system dynamics is understood as the Raman transitions described by the effective Hamiltonian

$$H_{\text{eff}} = \frac{1}{2} [c_0 \Omega_p |\mu_0\rangle + c_{2l} \Omega_s |\mu_{2l}\rangle] \langle E_0| + \text{h.c.}, \quad (15)$$

which is obtained by performing $e^{iH_0 t} H_D e^{-iH_0 t}$ and neglecting fast-oscillating terms under the rotating-wave approximation (see Supplementary Note 1 for more details). Hereafter, we omit the explicit g_c dependence of all the probability amplitudes c_k for simplicity. The dynamics governed by H_{eff} can be interpreted as a multi-photon down-conversion process (see Fig. 1a), with an efficiency controllable by the coefficients c_0 and c_{2l} . When the initial state is $|\mu_0\rangle$, the probability amplitude of the state $|\mu_{2l}\rangle$ at time t reads

$$P_{2l} = \frac{c_0 \Omega_p c_{2l} \Omega_s}{4\Xi^2} [\cos(\Xi t) - 1], \quad \text{with } \Xi^2 = \frac{1}{4} [(c_0 \Omega_p)^2 + (c_{2l} \Omega_s)^2]. \quad (16)$$

Choosing $t = \pi/\Xi$, the probability amplitude P_{2l} and the mean photon number of the system both reach their maximum values. Then, as long as $\Omega_p \neq 0$ and $\Omega_s \neq 0$, P_{2l} is measurable because c_0 and c_{2l} are significant. Accordingly, the theoretical prediction of the maximum photon number of the system after a finite-time

evolution is

$$\bar{n}_{\text{max}}^e = 2l|P_{2l}(t)|^2 = 2l \left| \frac{2c_0 \Omega_p c_{2l} \Omega_s}{(c_0 \Omega_p)^2 + (c_{2l} \Omega_s)^2} \right|^2. \quad (\text{where } t = \pi/\Xi) \quad (17)$$

However, when g_c is tuned across the critical point, the needed evolution time to achieve the maximum photon number tends infinite due to $\Xi \rightarrow 0$. To avoid such an infinite-time evolution, we impose $t \leq 10^6/\omega$ in this protocol when $\Xi \rightarrow 0$. In this limit, we obtain $P_{2l} \rightarrow 0$ because $\cos(\Xi t) \rightarrow 1$ according to Eq. (16). Therefore, as shown in Fig. 3, we theoretically predict a sudden change of the mean photon number when $g_c \rightarrow 1$, indicating the occurrence of the superradiant QPT.

This demonstration can be interpreted as a partial quantum process tomography, which starts at preparing the initial state $|\mu_0\rangle$ and fixing g_c to a specific value, e.g., $g_c = 0.999$. Then, turning on the drivings, one can detect the system dynamics (see the example in Fig. 4a). After the detection, the drives are turned off and the system is prepared to the state $|\mu_0\rangle$. The next step is tuning g_c to another value (e.g., $g_c = 1.001$) through adjusting the frequencies Ω and ω . Thus, after the energy spectrum of the system stabilizes, one can turn on the drivings again and detect the system dynamics (see the example in Fig. 4b). By repeating these processes, we can know the system dynamics for an arbitrary g_c and demonstrate the critical phenomenon as shown in Fig. 4c, which shows the maximum value \bar{n}_{max} of the mean photon number of the system in the evolution. Note that the mean photon number is no longer $\bar{n} = \langle a^\dagger a \rangle$, but $\bar{n} = \langle X^- X^+ \rangle$, where X^+ (X^-) is the positive (negative) frequency component of the quadrature operator $X = a + a^\dagger$ ^{7,8,42,43}. Otherwise, because of $\langle E_0 | a^\dagger a | E_0 \rangle \neq 0$, an observation of the stream of photons in the eigenstate $|E_0\rangle$ of the Rabi model would give rise to a perpetuum mobile behavior^{38,42}. Because these photons can be emitted and detected in a dissipative dynamics, a measurement of the population dynamics is not necessary.

Using the corresponding input-output theory^{39,43}, we apply

$$X^+ = \sum_{j,j'} \langle \xi_j | (a + a^\dagger) | \xi_j \rangle | \xi_j \rangle \langle \xi_j |, \quad (18)$$

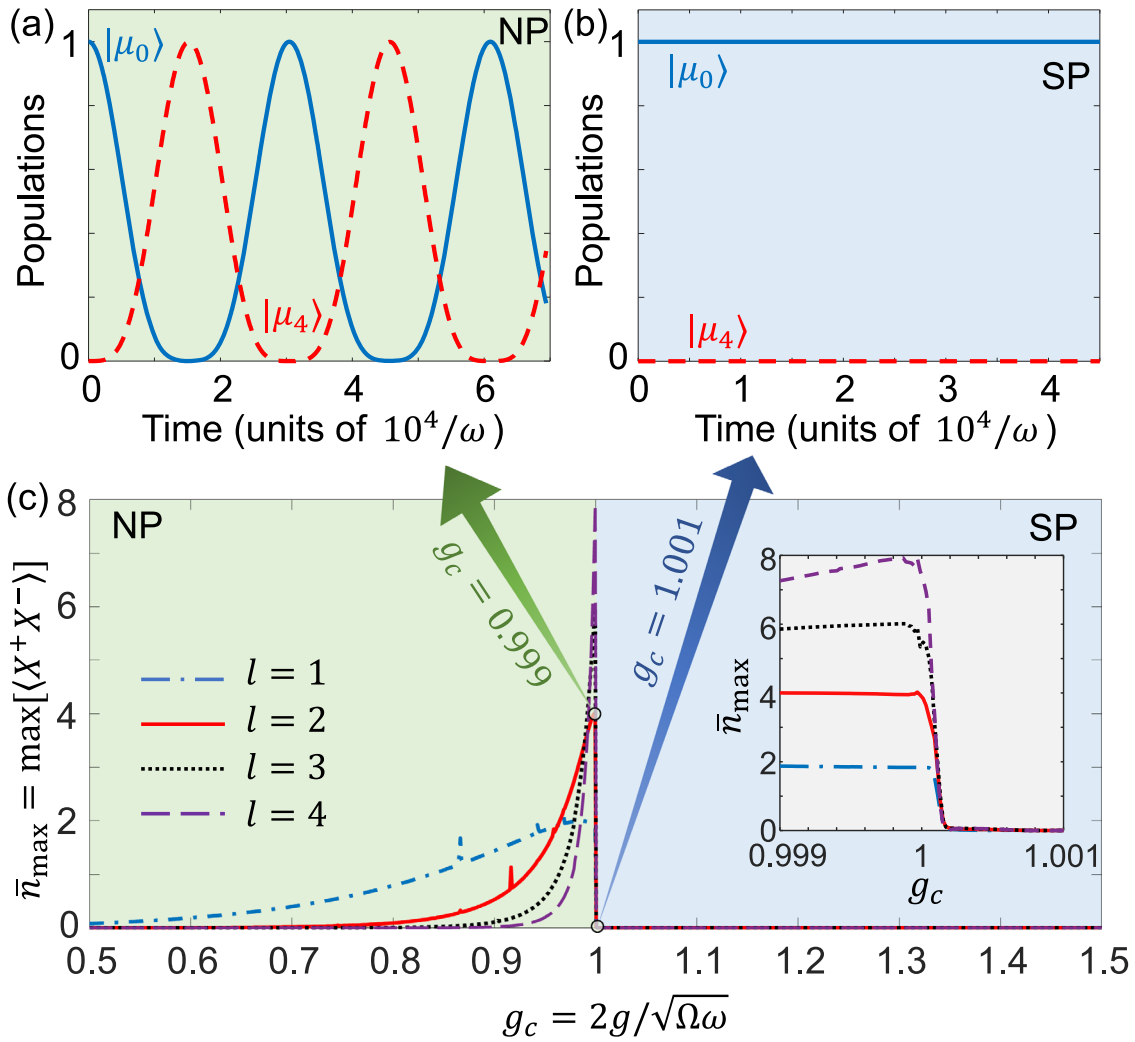


Fig. 4 Dynamics of the model. Populations of the ground state $|\mu_0\rangle$ and the four-photon state $|\mu_4\rangle$ in (a) the normal phase (NP, green-shaded area) for $g_c = 0.999$, and (b) the superradiant phase (SP, blue-shaded area) for $g_c = 1.001$, calculated for the total Hamiltonian $H_{\text{tot}} = H_0 + H_D$. **c** Maximum value (\bar{n}_{max} at the time $t = \pi/\Xi$) over time of the mean photon number in the evolution governed by H_{tot} for $l = 1, 2, 3, 4$. Parameters are the same as those in Fig. 3. Here, $n_d \geq l$ is used to tune the driving frequencies ω_p and ω_s ; and for simplicity, we choose $n_d = 2 + l$ in the simulation. The eigenvalues E_0 and E_2 can be numerically calculated. The level frequency ω_μ is chosen so that the state $|E_0\rangle$ is the highest level in the dynamical evolution and the state $|\mu\rangle$ is off-resonant to the cavity bare frequency. Thus, the system only has real cavity photons contributed by the state $|\mu_{2l}\rangle$.

and $X^- = (X^+)^\dagger$ with $j' < j$. Here, Eq. (18) describes that a photon emission from the cavity is associated with the transition from a high-energy eigenstate $|\xi_j\rangle$ to a low-energy eigenstate $|\xi_{j'}\rangle$ of H_0 . Note that in the subspace $\{|\mu_n\rangle\}$, we can obtain $\sum_n |\mu_n\rangle \langle \mu_n| X^+ \sum_m |\mu_m\rangle \langle \mu_m| = |\mu\rangle \langle \mu| \otimes a$. That is, the photons in the states $|\mu_{2l}\rangle$ are real cavity photons, thus,

$$X^- X^+ |\mu_{2l}\rangle \equiv |\mu\rangle \langle \mu| \otimes a^\dagger a |\mu_{2l}\rangle = a^\dagger a |2l\rangle |\mu\rangle. \quad (19)$$

Therefore, the system has maximum real photons at the time $t = \pi/\Xi$, when the state $|\mu_{2l}\rangle$ is maximally populated according to Eq. (16). Figure 4c shows that \bar{n}_{max} reaches a maximum when $g_c \rightarrow 1^-$, indicating a rapid increase of the mean photon number near the critical point. Then, when g_c is tuned across the critical point, the photons suddenly vanish. The inset of Fig. 4 shows such changes more clearly, where we can see that \bar{n}_{max} changes sharply when slightly increasing g_c from $g_c = 1$ to $g_c = (1 + 10^{-4})$, demonstrating a sudden change of the photon-number distributions in $|E_0\rangle$ (see also Supplementary Note 1). Obviously, the actual dynamics of the system shown in Fig. 4c

coincides very well with the effective one shown in Fig. 3. As an example for $l = 2$, when $g_c = 0.99999$, the theoretical prediction of the maximum photon number is $\bar{n}_{\text{max}}^e \simeq 3.89$, and the actual number is $\bar{n}_{\text{max}} \simeq 3.93$. When we change g_c to $g_c = 1.0003$, the theoretical prediction becomes $\bar{n}_{\text{max}}^e \simeq 0.0018 n^- \text{max} \simeq 0.0018$ and the actual number is $\bar{n}_{\text{max}} \simeq 0.04$. Both close to zero, indicating a sudden change of the mean photon number at the critical point. The sudden change in \bar{n}_{max} can be easily detected experimentally by measuring the rate of photons transmitted out of the cavity. Note that numerical results for actual dynamical evolution in this manuscript are obtained using the total Hamiltonian $H_{\text{tot}} = H_0 + H_D$ without approximations.

Output photon rate

A proper generalized input-output relation in the ultrastrong-coupling regime determines the output cavity photon rate^{38,39} by

$$\Phi_{\text{out}} = \kappa \text{Tr}[X^- X^+ \rho]. \quad (20)$$

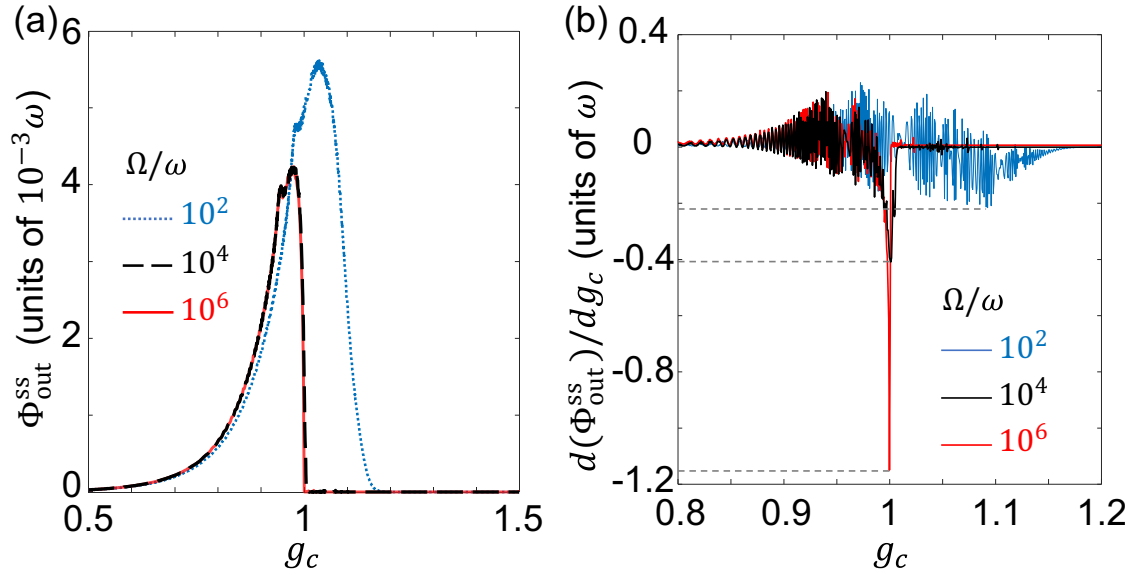


Fig. 5 Photon output field. **a** Steady-state output photon rates $\Phi_{\text{out}}^{\text{ss}} = \Phi_{\text{out}}|_{t \rightarrow \infty}$ defined in Eq. (20), and **(b)** the corresponding derivative $d(\Phi_{\text{out}}^{\text{ss}})/dg_c$ versus g_c for $l=2$. Dissipation rates are $\kappa = \gamma_1 = \gamma_2 = 0.01\omega$. We choose relatively strong driving fields, i.e., $\Omega_p = 0.05(E_2 - E_0)$ and $\Omega_s = 2\Omega_p$, to achieve relatively large output photon rates. Strong driving fields may cause small errors (via counter-rotating effects) in obtaining the effective Hamiltonian H_{eff} , leading to oscillations in $\Phi_{\text{out}}^{\text{ss}}$. These small errors do not affect the observation of the critical phenomenon, i.e., an extremum of $d(\Phi_{\text{out}}^{\text{ss}})/dg_c$ at $g_c \rightarrow 1^+$. The blue, black, and red curves are plotted using frequency ratios $\Omega/\omega = 10^2$, $\Omega/\omega = 10^4$, and $\Omega/\omega = 10^6$, respectively. Other parameters are the same as those in Fig. 4.

Here, κ is the cavity decay rate and ρ is the density matrix obeying the following master equation at zero temperature^{7,8},

$$\dot{\rho} = i[\rho, H_{\text{tot}}] + \sum_{\nu=1}^3 \sum_{j,j' < j} \Gamma_{jj'}^{(\nu)} \left\{ \mathcal{D}[\xi_j] \langle \xi_j | \rho \right\}, \quad (21)$$

where $H_{\text{tot}} = H_0 + H_D$ is the total Hamiltonian and

$$\mathcal{D}[o]\rho = o\rho o^\dagger - \frac{1}{2}(o^\dagger o \rho + \rho o^\dagger o), \quad (22)$$

is the Lindblad superoperator. The relaxation coefficients $\Gamma_{jj'}^{(\nu)}$ can be written in compact forms as

$$\begin{aligned} \Gamma_{jj'}^{(1)} &= \gamma_1 |\langle \xi_j | (|\mu\rangle \langle g| + |g\rangle \langle \mu|) | \xi_j \rangle|^2, \\ \Gamma_{jj'}^{(2)} &= \gamma_2 |\langle \xi_j | (|g\rangle \langle e| + |e\rangle \langle g|) | \xi_j \rangle|^2, \\ \Gamma_{jj'}^{(3)} &= \kappa |\langle \xi_j | (a + a^\dagger) | \xi_j \rangle|^2, \end{aligned} \quad (23)$$

where $\gamma_{1,(2)}$ is the spontaneous emission rate of the transition $|g\rangle \rightarrow |\mu\rangle$ ($|e\rangle \rightarrow |g\rangle$).

The steady-state output field can remain unchanged for a long time. This can reduce the difficulties in experiments to measure the emitted photons. Taking $l=2$ as an example, in Fig. 5a, we show the steady-state output photon rates $\Phi_{\text{out}}^{\text{ss}} = \Phi_{\text{out}}|_{t \rightarrow \infty}$, which is independent of the initial state. Focusing on $\Omega/\omega = 10^4$ (the black-solid curve in Fig. 5a), the peak value of steady-state output photon rate can reach $\Phi_{\text{out}}^{\text{ss}} \gtrsim 4 \times 10^{-3}\omega$ in the NP near the critical point when the dissipation rates are $\kappa = \gamma_1 = \gamma_2 = 0.01\omega$. We can choose $\omega \sim 2\pi \times 5\text{MHz}$ and $\Omega \sim 2\pi \times 50\text{GHz}$ ^{44,45}, the cavity can transmit $\sim 1.25 \times 10^5$ photons per second, which is detectable in cavity- and circuit-QED systems. The coupling strength is $g \sim 2\pi \times 250\text{MHz}$, and the driving amplitudes are $\Omega_p \gtrsim 2\pi \times 0.5\text{kHz}$ and $\Omega_s \gtrsim 2\pi \times 1\text{kHz}$, which are feasible in current experiments^{7,8,46–49}. When the parameter g_c crosses the critical point, suddenly there is no photon released from the cavity. This indicates the drastic change of the photon number distributions and the occurrence of the QPT. The curves in Fig. 5a coincide well with those in Fig. 2a, proving that the steady-state output field is a good signature of the superradiant QPT.

Finite-frequency effect

As mentioned above, for finite frequencies of Ω and ω , the higher-order terms $O(\omega g_c^2/\Omega)$ cannot be ideally neglected but modify the eigenvalues and eigenstates of H_R near the critical point. The influence of this finite-frequency effect is shown in Fig. 5. The first-order derivatives of $\Phi_{\text{out}}^{\text{ss}}$ versus g_c are shown in Fig. 5b. For $\Omega/\omega = 10^4$ (black-solid curve in Fig. 5b) and $\Omega/\omega = 10^6$ (red-solid curve in Fig. 5b), we can see deep thin dips near the critical point of $g_c = 1$, indicating the sudden changes of output photon rates. For $\Omega/\omega = 10^2$, the phenomenon becomes less pronounced (see the blue-solid curve in Fig. 5b).

Discussion

Our protocol does not need to control a parameter to adiabatically approach the critical point. Also, we do not need to prepare the equilibrium state, which is challenging in experiments because the time required diverges^{10,35}. The critical phenomenon can be translated to a sudden change of the output photon rate, which can be easily detected in experiments. Thus, our protocol could be efficient to observe the critical phenomenon of the sudden change of photon number distributions in a superradiant QPT. Moreover, unlike dissipative phase transitions^{19,24,25,50–52}, the drivings and dissipation in this manuscript are only used for quantum measurements and do not affect the QPT.

Our protocol could be implemented with superconducting circuits, which have realized the ultra- and deep-strong couplings between a single atom and a single-mode cavity^{44,45,53–57}. One can couple, e.g., a flux qubit^{7,8,46–49}, with a lumped-element resonator via Josephson junctions to reach a coupling strength of $g/2\pi \sim 1\text{GHz}$ ^{44,45}. To reduce the cavity frequency to $\omega = 2\pi \times 5\text{MHz}$, one can use an array of dc superconducting quantum interference devices⁵⁸ instead of the lumped-element resonator (see Supplementary Note 2). The level structure of the atom can be realized by adjusting the external magnetic flux through the qubit loop^{38,39,59}. Moreover, simulated quantum Rabi models^{7,8,60–65}, which work in the rotating frames of the Jaynes-Cummings models, can be another possible implementation of our protocol (see also Supplementary Note 3).

Conclusion

We have investigated a method to observe quantum critical phenomena: a sudden change of photon number distributions in a quantum phase transition exhibited by the quantum Rabi model. We can interpret the system dynamics as a multi-photon down-conversion process and study the outputs near the critical point. When the normalized coupling strength g_c is tuned across the critical point, the output of the system changes abruptly. This reflects a sudden change of the eigenstate $|E_0\rangle$ of the quantum Rabi model. Specifically, for the Rabi Hamiltonian in the NP, a pump pulse can be converted into a Stokes pulse and multiple cavity photons, while in the SP, it cannot. One can observe such a change by measuring the photons emitted out of the cavity continuously in the steady state. Moreover, for finite frequencies, we demonstrate that a small frequency ratio Ω/ω may lead to the disappearance of the critical phenomenon. We expect that our method can provide a useful tool to study various critical phenomena exhibited by quantum phase transitions without preparing their equilibrium states.

Data availability

The data used for obtaining the presented numerical results as well as for generating the plots is available on request. Please refer to yehong.chen@fzu.edu.cn.

Received: 25 March 2023; Accepted: 8 November 2023;

Published online: 05 January 2024

References

- Agarwal, G. S. *Quantum Optics*. (Cambridge University Press, Cambridge, England, 2012).
- Scully, M. O. & Zubairy, M. S. *Quantum Optics*. (Cambridge University Press, Cambridge, England, 1997).
- Scully, M. O. & Svidzinsky, A. A. The super of superradiance. *Science* **325**, 1510–1511 (2009).
- Sachdev, S. *Quantum Phase Transitions*. (Cambridge University Press, Cambridge, England, 2011).
- Cong, K. et al. Dicke superradiance in solids [invited]. *J. Opt. Soc. Am. B* **33**, C80 (2016).
- Kirton, P., Roses, M. M., Keeling, J. & Torre, E. G. D. Introduction to the Dicke model: From equilibrium to nonequilibrium, and viceversa. *Adv. Quant. Tech.* **2**, 1800043 (2018).
- Kockum, A. F., Miranowicz, A., Liberato, S. D., Savasta, S. & Nori, F. Ultrastrong coupling between light and matter. *Nat. Rev. Phys.* **1**, 19–40 (2019).
- Forn-Díaz, P., Lamata, L., Rico, E., Kono, J. & Solano, E. Ultrastrong coupling regimes of light-matter interaction. *Rev. Mod. Phys.* **91**, 025005 (2019).
- Ashhab, S. Superradiance transition in a system with a single qubit and a single oscillator. *Phys. Rev. A* **87**, 013826 (2013).
- Hwang, M.-J., Puebla, R. & Plenio, M. B. Quantum phase transition and universal dynamics in the Rabi model. *Phys. Rev. Lett.* **115**, 180404 (2015).
- Hepp, K. & Lieb, E. H. On the superradiant phase transition for molecules in a quantized radiation field: the Dicke maser model. *Ann. Phys.* **76**, 360–404 (1973).
- Wang, Y. K. & Hioe, F. T. Phase transition in the Dicke model of superradiance. *Phys. Rev. A* **7**, 831–836 (1973).
- Emary, C. & Brandes, T. Quantum chaos triggered by precursors of a quantum phase transition: The Dicke model. *Phys. Rev. Lett.* **90**, 044101 (2003).
- Lambert, N., Emary, C. & Brandes, T. Entanglement and the phase transition in single-mode superradiance. *Phys. Rev. Lett.* **92**, 073602 (2004).
- Scully, M. O. Single photon subradiance: Quantum control of spontaneous emission and ultrafast readout. *Phys. Rev. Lett.* **115**, 243602 (2015).
- Shammah, N. et al. Superradiance with local phase-breaking effects. *Phys. Rev. A* **96**, 023863 (2017).
- Shammah, N. et al. Open quantum systems with local and collective incoherent processes: Efficient numerical simulations using permutational invariance. *Phys. Rev. A* **98**, 063815 (2018).
- Makihara, T. et al. Ultrastrong magnon–magnon coupling dominated by antiresonant interactions. *Nat. Commun.* **12**, 3115 (2021).
- Baumann, K., Guerlin, C., Brennecke, F. & Esslinger, T. Dicke quantum phase transition with a superfluid gas in an optical cavity. *Nature* **464**, 1301–1306 (2010).
- Baumann, K., Mottl, R., Brennecke, F. & Esslinger, T. Exploring symmetry breaking at the Dicke quantum phase transition. *Phys. Rev. Lett.* **107**, 140402 (2011).
- Bastidas, V. M., Emary, C., Regler, B. & Brandes, T. Nonequilibrium quantum phase transitions in the Dicke model. *Phys. Rev. Lett.* **108**, 043003 (2012).
- Mlynek, J. A., Abdumalikov, A. A., Eichler, C. & Wallraff, A. Observation of Dicke superradiance for two artificial atoms in a cavity with high decay rate. *Nat. Commun.* **5**, 5186 (2014).
- Fuchs, S., Ankerhold, J., Blencowe, M. & Kubala, B. Non-equilibrium dynamics of the Dicke model for mesoscopic aggregates: signatures of superradiance. *J. Phys. B* **49**, 035501 (2016).
- Zhang, Z. et al. Nonequilibrium phase transition in a spin-1 Dicke model. *Optica* **4**, 424 (2017).
- Léonard, J., Morales, A., Zupancic, P., Esslinger, T. & Donner, T. Supersolid formation in a quantum gas breaking a continuous translational symmetry. *Nature* **543**, 87–90 (2017).
- Zhu, C. J., Ping, L. L., Yang, Y. P. & Agarwal, G. S. Squeezed light induced symmetry breaking superradiant phase transition. *Phys. Rev. Lett.* **124**, 073602 (2020).
- Cai, M.-L. et al. Observation of a quantum phase transition in the quantum Rabi model with a single trapped ion. *Nat. Commun.* **12**, 1126 (2021).
- Chen, X. et al. Experimental quantum simulation of superradiant phase transition beyond no-go theorem via antisqueezing. *Nat. Commun.* **12**, 6281 (2021).
- Puebla, R., Hwang, M.-J. & Plenio, M. B. Excited-state quantum phase transition in the Rabi model. *Phys. Rev. A* **94**, 023835 (2016).
- Shen, L.-T., Yang, Z.-B., Wu, H.-Z. & Zheng, S.-B. Quantum phase transition and quench dynamics in the anisotropic Rabi model. *Phys. Rev. A* **95**, 013819 (2017).
- Liu, M. et al. Universal scaling and critical exponents of the anisotropic quantum Rabi model. *Phys. Rev. Lett.* **119**, 220601 (2017).
- Hwang, M.-J., Rabl, P. & Plenio, M. B. Dissipative phase transition in the open quantum Rabi model. *Phys. Rev. A* **97**, 013825 (2018).
- Jiang, X. et al. Universal dynamics of the superradiant phase transition in the anisotropic quantum Rabi model. *Phys. Rev. A* **104**, 043307 (2021).
- Zheng, R.-H. et al. Observation of a superradiant phase transition with emergent cat states. *Phys. Rev. Lett.* **131**, 113601 (2023).
- Garbe, L., Bina, M., Keller, A., Paris, M. G. A. & Felicetti, S. Critical quantum metrology with a finite-component quantum phase transition. *Phys. Rev. Lett.* **124**, 120504 (2020).
- Tsang, M. Quantum transition-edge detectors. *Phys. Rev. A* **88**, 021801(R) (2013).
- Wang, T.-L. et al. Quantum Fisher information as a signature of the superradiant quantum phase transition. *N. J. Phys.* **16**, 063039 (2014).
- Stassi, R., Ridolfo, A., Di Stefano, O., Hartmann, M. J. & Savasta, S. Spontaneous conversion from virtual to real photons in the ultrastrong-coupling regime. *Phys. Rev. Lett.* **110**, 243601 (2013).
- Huang, J.-F. & Law, C. K. Photon emission via vacuum-dressed intermediate states under ultrastrong coupling. *Phys. Rev. A* **89**, 033827 (2014).
- Kockum, A. F. et al. Deterministic quantum nonlinear optics with single atoms and virtual photons. *Phys. Rev. A* **95**, 063849 (2017).
- Chen, Y.-H. et al. Fast binomial-code holonomic quantum computation with ultrastrong light-matter coupling. *Phys. Rev. Res.* **3**, 033275 (2021).
- Ciuti, C. & Carusotto, I. Input-output theory of cavities in the ultrastrong coupling regime: The case of time-independent cavity parameters. *Phys. Rev. A* **74**, 033811 (2006).
- Ridolfo, A., Leib, M., Savasta, S. & Hartmann, M. J. Photon blockade in the ultrastrong coupling regime. *Phys. Rev. Lett.* **109**, 193602 (2012).
- Yoshihara, F. et al. Superconducting qubit–oscillator circuit beyond the ultrastrong-coupling regime. *Nat. Phys.* **13**, 44–47 (2016).
- Chen, Z. et al. Single-photon-driven high-order sideband transitions in an ultrastrongly coupled circuit-quantum-electrodynamics system. *Phys. Rev. A* **96**, 012325 (2017).
- Gu, X. et al. Microwave photonics with superconducting quantum circuits. *Phys. Rep.* **718–719**, 1–102 (2017).
- Krantz, P. et al. A quantum engineer’s guide to superconducting qubits. *Appl. Phys. Rev.* **6**, 021318 (2019).
- Kjaergaard, M. et al. Superconducting qubits: Current state of play. *Ann. Rev. Cond. Mat. Phys.* **11**, 369–395 (2020).
- Kwon, S., Tomonaga, A., Bhai, G. L., Devitt, S. J. & Tsai, J.-S. Gate-based superconducting quantum computing. *J. Appl. Phys.* **129**, 041102 (2021).
- Klinger, J., Kessler, H., Wolke, M., Mathey, L. & Hemmerich, A. Dynamical phase transition in the open Dicke model. *Proc. Nat. Acad. Sci.* **112**, 3290–3295 (2015).

51. Minganti, F. et al. Continuous dissipative phase transitions with or without symmetry breaking. *N. J. Phys.* **23**, 122001 (2021).
52. Minganti, F. et al. Liouvillian spectral collapse in the Scully-Lamb laser model. *Phys. Rev. Res.* **3**, 043197 (2021).
53. Niemczyk, T. et al. Circuit quantum electrodynamics in the ultrastrong-coupling regime. *Nat. Phys.* **6**, 772–776 (2010).
54. Forn-Diaz, P. et al. Observation of the Bloch-Siegert shift in a qubit-oscillator system in the ultrastrong coupling regime. *Phys. Rev. Lett.* **105**, 237001 (2010).
55. Yoshihara, F. et al. Characteristic spectra of circuit quantum electrodynamics systems from the ultrastrong- to the deep-strong-coupling regime. *Phys. Rev. A* **95**, 053824 (2017).
56. Bosman, S. J. et al. Multi-mode ultra-strong coupling in circuit quantum electrodynamics. *npj Quant. Info.* **3**, 46 (2017).
57. Yoshihara, F. et al. Inversion of qubit energy levels in qubit-oscillator circuits in the deep-strong-coupling regime. *Phys. Rev. Lett.* **120**, 183601 (2018).
58. Liao, J.-Q. et al. Controlling the transport of single photons by tuning the frequency of either one or two cavities in an array of coupled cavities. *Phys. Rev. A* **81**, 042304 (2010).
59. Stefano, O. D. et al. Feynman-diagrams approach to the quantum Rabi model for ultrastrong cavity QED: stimulated emission and reabsorption of virtual particles dressing a physical excitation. *N. J. Phys.* **19**, 053010 (2017).
60. Ballester, D., Romero, G., García-Ripoll, J. J., Deppe, F. & Solano, E. Quantum simulation of the ultrastrong-coupling dynamics in circuit quantum electrodynamics. *Phys. Rev. X* **2**, 021007 (2012).
61. Lv, D. et al. Quantum simulation of the quantum Rabi model in a trapped ion. *Phys. Rev. X* **8**, 021027 (2018).
62. Qin, W. et al. Exponentially enhanced light-matter interaction, cooperativities, and steady-state entanglement using parametric amplification. *Phys. Rev. Lett.* **120**, 093601 (2018).
63. Leroux, C., Govia, L. C. G. & Clerk, A. A. Enhancing cavity quantum electrodynamics via antisqueezing: Synthetic ultrastrong coupling. *Phys. Rev. Lett.* **120**, 093602 (2018).
64. Sánchez Muñoz, C. et al. Simulating ultrastrong-coupling processes breaking parity conservation in Jaynes-Cummings systems. *Phys. Rev. A* **102**, 033716 (2020).
65. Chen, Y.-H. et al. Shortcuts to adiabaticity for the quantum Rabi model: Efficient generation of giant entangled cat states via parametric amplification. *Phys. Rev. Lett.* **126**, 023602 (2021).

Acknowledgements

Y.-H.C. was supported by the National Natural Science Foundation of China under Grant No. 12304390. A.M. was supported by the Polish National Science Centre (NCN) under the Maestro Grant No. DEC-2019/34/A/ST2/00081. W.Q. was supported in part by the Incentive Research Project of RIKEN. Y.X. was supported by the National Natural Science Foundation of China under Grant No. 11575045, the Natural Science Funds for

Distinguished Young Scholar of Fujian Province under Grant 2020J06011 and Project from Fuzhou University under Grant JG202001-2. F.N. is supported in part by: Nippon Telegraph and Telephone Corporation (NTT) Research, the Japan Science and Technology Agency (JST) [via the Quantum Leap Flagship Program (Q-LEAP), and the Moonshot R&D Grant Number JPMJMS2061], the Asian Office of Aerospace Research and Development (AOARD) (via Grant No. FA2386-20-1-4069), and the Office of Naval Research (ONR).

Author contributions

Y.-H.C. conceived and developed the idea. Y.Q., A.M., N.L. and R.S. analyzed the data and performed the numerical simulations, with help from S.-B.Z. and W.Q.Y.-H.C., Y.X. and F.N. cowrote the paper with feedback from all authors.

Competing interests

The authors declare no competing interests.

Additional information

Supplementary information The online version contains supplementary material available at <https://doi.org/10.1038/s42005-023-01457-w>.

Correspondence and requests for materials should be addressed to Ye-Hong Chen, Yan Xia or Franco Nori.

Peer review information *Communications Physics* thanks the anonymous reviewers for their contribution to the peer review of this work.

Reprints and permission information is available at <http://www.nature.com/reprints>

Publisher's note Springer Nature remains neutral with regard to jurisdictional claims in published maps and institutional affiliations.



Open Access This article is licensed under a Creative Commons Attribution 4.0 International License, which permits use, sharing, adaptation, distribution and reproduction in any medium or format, as long as you give appropriate credit to the original author(s) and the source, provide a link to the Creative Commons licence, and indicate if changes were made. The images or other third party material in this article are included in the article's Creative Commons licence, unless indicated otherwise in a credit line to the material. If material is not included in the article's Creative Commons licence and your intended use is not permitted by statutory regulation or exceeds the permitted use, you will need to obtain permission directly from the copyright holder. To view a copy of this licence, visit <http://creativecommons.org/licenses/by/4.0/>.

© The Author(s) 2024